Ground Moving Target Trajectory Reconstruction in Single-Channel Circular SAR

J.B. Poisson, *Student Member, IEEE*, H. Oriot, and F. Tupin, *Senior Member, IEEE*

***Abstract*—Synthetic aperture radar has become an important technique for generating high-resolution images of the ground, because of its all-weather capabilities. SAR imaging of stationary scenes is nowadays well mastered. Moving targets induce a delocalization and a defocusing effect in the azimuth direction in a SAR image. This latter effect can be used to detect moving targets, to image them and to estimate their azimuthal velocity, but the main limitation is the impossibility to estimate the full target velocity vector, because of the Doppler shift dependency on azimuthal position and radial velocity.**

In this paper, we analyse the performances of a method that reconstructs the real target trajectory given the apparent positions of the moving target measured on SAR images acquired along a circular trajectory. We first outline the steps of this trajectory reconstruction methodology, then we perform a mathematical analysis of this methodology and finally we present some results on real data, around two French cities.

Index terms – circular SAR, moving target, trajectory reconstruction, focusing

I. Introduction

Synthetic aperture radar has become an important technique for generating high-resolution images of the ground, because of its all-weather capabilities. SAR imaging of stationary scenes is nowadays well mastered [1] but if a moving target is present in the illuminated scene, it appears delocalized in the azimuth direction and defocused in the SAR image [2].

Two main processing categories have been considered in the recent literature. The first category concerns multisensor (or multichannel) techniques [3]. This category mainly relies on Displaced Phase Center Antenna (DPCA) [4], Space-Time adaptive processing (STAP) [5, 6] and along track interferometry (ATI) [7]. STAP and DPCA are applied to non-focused data and enable to detect and estimate the moving targets radial velocity. The azimuth velocity is then estimated by filtering. ATI or AT-InSAR [8] is applied to SAR data and enable detect and estimate the moving target radial velocity vector, the azimuthal velocity being estimated by refocusing. However, it is difficult to reconstruct the target trajectory, because the signals are integrated over a long time. One advantage of these multisensor techniques is the ability to suppress clutter. The moving target detection is therefore made easier, especially in severe background environment [9, 10]. For practical reasons, a significant part of airborne SAR systems is limited to one single channel. The SAR systems developed by the French Aerospace Lab ONERA (SETHI [11], and more recently RAMSES NG [12]) fit into this category. Standard single antenna processing exploits the moving target apparent characteristics to focus them [13, 14] and estimate their azimuth velocity [15] under the assumption of a high PRF, in order to avoid the Doppler ambiguity problem [16]. The main limitations of these methods are:

1) The difficulty to estimate the full target velocity vector, because of the Doppler shift dependence on both azimuthal position and radial velocity of the moving target [17-19].

2) The errors in the azimuthal velocity estimate due to the background image [13].

Some interesting studies have been done on ground moving target tracking in single channel SAR to solve these problems. Kirscht [20] has worked on moving target detection and apparent trajectory estimation. He uses the information content of multilook processing [21] to detect potential moving targets. The apparent target velocity vector is then estimated from target displacement between successive images with a normalized cross correlation function as matching criterion [22]. Dias and Marques [23] have worked on real trajectory reconstruction by using the amplitude modulation term of the returned echo from a moving target to estimate its radial velocity, and then avoid the azimuth ambiguity. The radial velocity estimator used in [23] yields effective results for a high signal-to-clutter (SCR) ratio (14 dB). Itoh [24] has worked on moving target radial motion estimation by Doppler detection, and has obtained effective results on ships. However, the radial velocity estimation given the antenna radiation pattern [23] or the centroid Doppler signature [24] may be affected by the clutter, the moving target anisotropic behaviour and the weak directivity of the beam. Furthermore, the velocity estimation with a cross correlation function [20, 22] could be imprecise in the case of defocused targets and the moving target trajectory estimation can thus be flawed. Therefore, the literature shows that it is difficult to reconstruct precisely the real moving target trajectory using monosensor SAR.

Acquisitions of SAR data over a circular trajectory [25] bring new information, because objects may be seen from

J. B. Poisson is with ONERA, The French Aerospace Lab, Palaiseau, France (e-mail: jean-baptiste.poisson@onera.fr).

H. Oriot is with ONERA, The French Aerospace Lab, Palaiseau, France (e-mail: helene.oriot@onera.fr).

F. Tupin is with the Laboratoire de Traitement et Communication de l'Information (LTCI), Telecom ParisTech, Paris, France. (e-mail: Florence.tupin@telecom-paristech.fr).

any aspect angle. The continuity of the SAR-platform movement may thus enhance moving targets trajectory reconstruction, because objects of interest may be seen during a longer time than in the linear stripmap SAR case. Thanks to the multiple azimuth direction, the azimuth ambiguity may be solved. Perlovsky [26] has used circular acquisition to work on moving target detection and trajectory reconstruction. He has proposed a method using multiple backprojection images as input of a framework called Dynamic Logic. This framework computes the conditional likelihood of the data values given the tested Gaussian models, providing moving target detection and characterization.

In this paper, we analyse performance of the reconstruction of the real target trajectory given the apparent positions of the moving target measured on SAR images acquired along a circular trajectory. We suppose that targets have already been detected (using, for instance, the method described in [27] or in [20]). In practice, we first manually detect the moving target on SAR images. These manual detections combined with a refocusing algorithm provide measurements of the apparent coordinates of the moving targets [28]. We use SAR images acquired along a circular trajectory to exploit the multiplicity of aspect angles and the long observation time, and we present an inversion method to validate the possibility of target trajectory reconstruction using single-channel circular SAR. This paper is organized as follows. In section II we present the data sets. In section III we outline the steps of our trajectory reconstruction methodology. In section IV we perform a mathematical analysis given synthetic data, we present in section V some trajectory reconstruction results on real data, around the city of Nîmes (acquired by the SAR system SETHI) and around the Istres Airport (acquired with RAMSES NG) in France and finally, we present in section VI some reconstruction results with an orientation constraint given by the road network.

II. PRESENTATION OF THE DATA SETS

The data were acquired with two different sensors from ONERA. The RAMSES NG sensor [12] is dedicated to defense and security applications. The main improvement is the ability to operate at long range and ultra-high resolution in X band. One dataset was acquired on Istres area in 2012 in X band with a 50 cm slant range resolution. We study a moving target (see Fig. 1) with ground truth (GPS data). The vehicle is a Renault Master with an average speed of $4m.s^{-1}$.

The SETHI sensor [11] is an airborne radar dedicated to civilian applications, equipped with different bands (P, L, X) on a Falcon 20. In this paper, we focus on the X dataset acquired around the city of Nîmes in 2009, with a 12 cm slant range resolution. We particularly examine a moving target with unknown trajectory which is supposed to be a train: we see several horizontal lines probably due to train cars. The residual curvature of the horizontal lines is due to range migration, which appears on images with high azimuth resolution (see Fig. 1). The main characteristics of the two acquisitions are summarized in Table I.

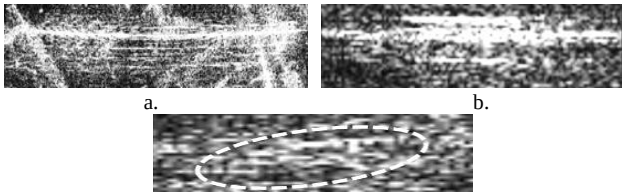

a. b.

c.

Fig. 1. Examples of signatures of moving targets on SAR images in the cities of Nîmes (a.) and Istres (b. and c.). The azimuth direction is horizontal so the defocusing effect appears as horizontal lines, with a residual curvature in the range direction for the train (a.). For c., the SCR is about 3dB, which is considered to be the limit for manual detection (the highest measured SCR value for this target is about 12dB).

TABLE I
AIRCRAFT TRAJECTORY PARAMETERS FOR NIMES (SETHI) AND ISTRES (RAMES NG)

Symbol	Quantity	Value
	Acquisition around the city of Nîmes	
NR	Near Range	$3700\ m$
ρ_r	Range resolution	$0.12\ cm$
V_S	Average sensor velocity	$\cong 130\ m.s^{-1}$
λ	Center wavelength	$3\ cm$
inc	Incidence	60°
Δt	Time interval between two images	$2s$
	Acquisition around the city of Istres	
NR	Near Range	$5500\ m$
ρ_r	Range resolution	$0.30\ cm$
V_S	Average sensor velocity	$\cong 120\ m.s^{-1}$
λ	Center wavelength	$3\ cm$
inc	Incidence	60°
Δt	Time interval between two images	$1s$

III. MOVING TARGET TRACKING METHODOLOGY

In this section, we present the moving target model, we describe the measurement method, we explain how the whole trajectory of the moving target is reconstructed given its apparent coordinates in the SAR images and under several moving target hypotheses, and then we present the system inversion calculation using the Least Mean Squares (LMS) method.

A. Moving target 2nd order model

Let us consider the SAR scenario illustrated in Fig. 2 where the SAR platform moves along a circular trajectory, so that SAR images can be computed for all possible azimuth angles. Images are processed in a spotlight mode, so each azimuth direction corresponds to a squint angle.

We consider a moving target P with velocity $\vec{V}$ and acceleration $\vec{A}$, which is considered to be constant during the sensor displacement between M_0 and M_t. The SAR-platform velocity is noted $\overrightarrow{V_S}$ and its acceleration is noted $\overrightarrow{A_S}$. In this section, we consider that the moving target is a point-like isotropic scatterer for the target phase history calculation. Real moving targets are actually made up of finite number of bright spots, whose spatial distributions are unpredictable, and depend on the target nature and on the aspect angle. However, for small integration angles, the point-like isotropic scatterer is a good approximation for moving targets. The method used to calculate the moving target phase history is given by [2] and explained here to present our notations.

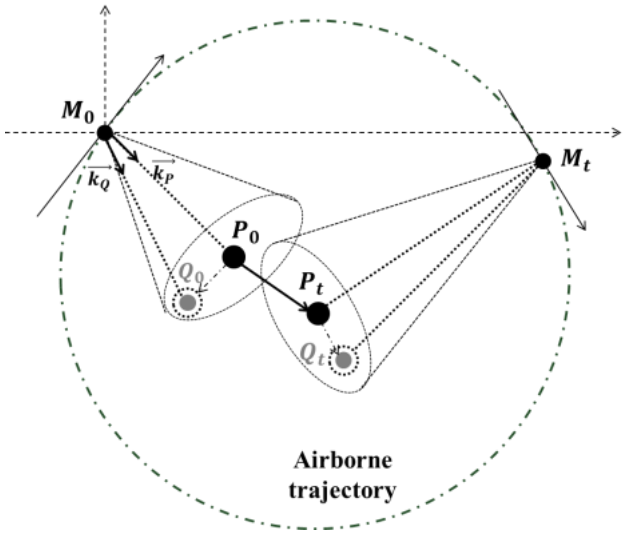

Fig. 2. Principle of calculation of two different images. For the first image (resp. the second), the SAR-platform is in M_0 (resp. in M_t) and the moving target is in P_0 (resp. in P_t). Q is a still target which appears at the same position as P (due to effects of target motion) on the SAR image.

At time t_0 (resp $t_0+\delta t$), the target is at position P_0 (resp. P_t, see Fig. 2). The phase of the returned echo $\delta\varphi_P$ during the time period δt is given by:

$$\delta\varphi_P = \frac{4\pi}{\lambda}\left(\left\|\overrightarrow{M_tP_t}\right\| - \left\|\overrightarrow{M_0P_0}\right\|\right) \tag{1}$$

Let

$$\overrightarrow{k_p} = \frac{\overrightarrow{M_0P_0}}{\left\|\overrightarrow{M_0P_0}\right\|} \tag{2}$$

be the normalized line of sight (LOS) vector for moving target P at time t_0. We also define $D_0 = \left\|\overrightarrow{M_0P_0}\right\|$ the distance between the SAR sensor and the moving target at time t_0. A development to the second order in δt is done, because most of the phase error due to target motion is given by second order terms [13]. For high order studies, see [10]. Adapting the range variation expression with time given by [2] to the circular flight path case, we have, before SAR processing:

$$\delta\varphi_P = \frac{4\pi}{\lambda}(\Lambda\delta t^2 + \Omega\delta t) \tag{3}$$

With:

$$\begin{aligned}\Lambda(V,A) &= \frac{V^2 + {V_S}^2}{2D_0} - \frac{\overrightarrow{V_S}.\vec{V}}{D_0} + \frac{\overrightarrow{k_p}}{2}.\left(\vec{A} - \overrightarrow{A_S}\right) - \frac{\left(\overrightarrow{V_S}.\overrightarrow{k_p}\right)^2}{2D_0} \\ &\quad - \frac{\left(\overrightarrow{k_p}.\vec{V}\right)^2}{2D_0} + \frac{1}{D_0}\left(\overrightarrow{V_S}.\overrightarrow{k_p} \times \overrightarrow{k_p}.\vec{V}\right)\end{aligned} \tag{4}$$

$$\Omega(V) = \overrightarrow{k_p}.\vec{V} - \overrightarrow{V_S}.\overrightarrow{k_p} \tag{5}$$

Where V is the magnitude of $\vec{V}$ and A is the magnitude of $\vec{A}$. V_S is the magnitude of the SAR-platform velocity $\overrightarrow{V_S}$. $\Omega(V)$ is a phase slope in the azimuth frequency domain that induces the azimuth shift of the target. The moving target P appears at the same position as a still target Q on the SAR image. So when we compute the azimuthal spectrum of the moving target P after SAR processing, the residual phase $\delta\varphi$ is the difference between the phase history of the moving target P and the phase history of the still target Q. Given $\overrightarrow{k_Q} = \overrightarrow{M_0Q}/\left\|\overrightarrow{M_0P_0}\right\|$, we thus have:

$$\delta\varphi = \delta\varphi_P - \delta\varphi_Q = \frac{4\pi}{\lambda}(\alpha\delta t^2 + \beta\delta t) \tag{6}$$

With α the defocusing parameter (see section II), given by:

$$\alpha(V,A) = \frac{V^2}{2D_0} - \frac{\overrightarrow{V_S}.\vec{V}}{D_0} + \frac{\overrightarrow{k_p}}{2}.\left(\vec{A} - \overrightarrow{A_S}\right) \tag{7}$$

And:

$$\beta(V) = \left(\Omega(V) + \overrightarrow{V_S}.\overrightarrow{k_Q}\right) \tag{8}$$

The difference of squint angles between P and Q is zero, so the difference of slope of the phase history is zero ($\beta = 0$), which leads to the relationship:

$$sin(\theta_P) = sin\left(\theta_Q\right) + \frac{\overrightarrow{k_P}.\vec{V}}{V_S} \tag{9}$$

Where θ_P (resp. θ_Q) is the squint angle for the moving target P (resp. for the still target Q). It should be noted that θ_Q is linked to the azimuth pixel line corresponding to the center of the target on the image.

Besides, α is an expression which is function of both the velocity and the acceleration of the moving target, especially the azimuth velocity ($\overrightarrow{V_S}.\vec{V}$) and the radial acceleration ($\vec{A}.\overrightarrow{k_P}$). Finally the ground moving target P appears on a SAR image at the apparent position $\left(D_0, \theta_Q\right)$ corresponding to pixel (i,j) in the SAR image, with the defocusing parameter α. These three measurements lead to the following system:

$$\begin{cases} \left\|\overrightarrow{M_0P_0}\right\| - D_0 = 0 \\ \overrightarrow{M_0P_0}.\vec{V} - D_0.V\left(sin\left(\theta_Q\right) + \dfrac{\overrightarrow{k_P}.\vec{V}}{V_S}\right) = 0 \\ \alpha - \left(\dfrac{V^2}{2D_0} - \dfrac{\overrightarrow{V_S}.\vec{V}}{D_0} + \dfrac{\vec{A}.\overrightarrow{k_P}}{2} + \dfrac{\gamma}{2}\right) = 0 \end{cases} \tag{10}$$

With $\gamma = \overrightarrow{\boldsymbol{A_S}}.\left(\overrightarrow{\boldsymbol{k_Q}} - \overrightarrow{\boldsymbol{k_p}}\right)$. Due to the number of unknowns, we need at least two sets of equations to solve the problem. A general overview of the model implementation is given in [29]. From now on the system unknowns will be expressed in the Cartesian system $(\mathbf{0}, \vec{\boldsymbol{x}}, \vec{\boldsymbol{y}})$, the $\vec{\boldsymbol{x}}$ axis representing the East direction and the $\vec{\boldsymbol{y}}$ axis representing the North direction.

B. Description of the measurements

As stated in the introduction, the main purpose of this paper is to analyse the algorithm that transforms the apparent measurements of the target into a geolocalised trajectory. The moving target detection step is therefore done by an operator:

the operator roughly points at the target on each image so that the input of the algorithm is a set of patches containing the moving target signature (see Fig. 1).

The estimation of the apparent position (i,j) of the target on the image as well as the estimation of the defocusing parameter (α) inside each patch is automatic: in order to measure α, we use the method described in [28] which is close to [19]: the moving target azimuthal spectrum is computed. As the target phase history is developed to the second order, we fit a parabola to its phase behavior. We then use an autofocus algorithm, based on a sharpness ratio measurement, which selects the best phase correction, *i. e.* which selects the value of α that best refocuses the moving target on the image. Finally, the moving target 2D centroid of magnitude image is computed to estimate the apparent coordinates (i,j) of the moving target center. Fig. 3 and Fig. 4 show the results of the measurement method on two signatures of the Renault Master presented in Fig. 1, with different SCR ratio. As a moving target generally appears on several images, we obtain a set of measurements used to reconstruct the real trajectory of the moving target.

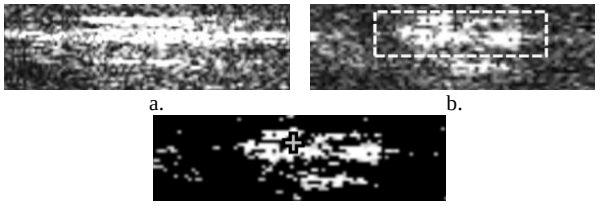

Fig. 3. Result of the measurement method on a signature of a moving target in Istres (SCR=10dB). a: defocused target (starting point). b: result of the focusing algorithm. The length of the moving target (highlighted in red) is about 6m, which corresponds to the length of a Renault Master. c.: result of the barycentric method for estimating the coordinates of the moving target center.

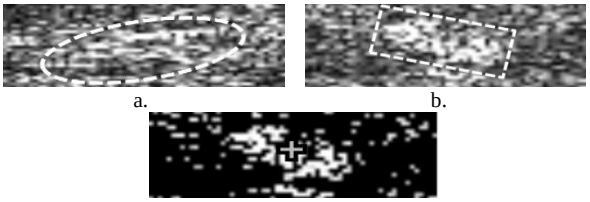

Fig. 4. Result of the measurement method on a signature of a moving target in Istres (SCR=3dB). a: defocused target (starting point). b: result of the focusing algorithm. c.: result of the barycentric method.

C. Moving target trajectory reconstruction methodology

Suppose that SAR images are computed every $\Delta\theta$ angle corresponding to a time interval ΔT. We propose to define a moving target model with constant acceleration during the time $N\Delta T$, N being the number of images used. Moreover, we consider that the target velocity and acceleration are collinear, so we look for targets moving along a straight line during calculation time. The moving target orientation is noted θ_{target}. Using this hypothesis, the ground coordinates of the moving target on each image #k can be written as:

$$\begin{cases} X_k = X + V\cos\theta_{target}k\Delta T + \frac{1}{2}A\cos\theta_{target}(k\Delta T)^2 \\ Y_k = Y + V\sin\theta_{target}k\Delta T + \frac{1}{2}A\sin\theta_{target}(k\Delta T)^2 \end{cases} \quad (11)$$

and we can use the system (10) for all the images between t_0 and $t_0+N\Delta T$ to obtain the target parameter vector $(X,Y,V,A,\theta_{target})$. By propagating this principle along the entire circular trajectory (see Fig. 5) of the SAR platform, we can reconstruct the whole trajectory of the moving target.

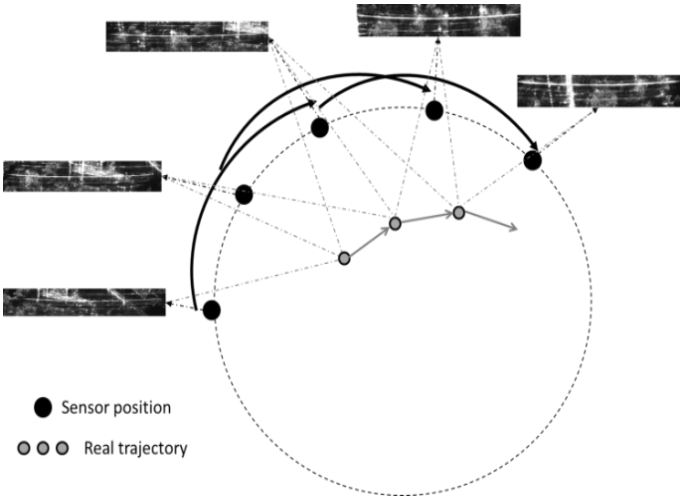

Fig. 5. Principle of reconstruction of the moving target whole trajectory. In this example, calculations of the moving target positions are made up of three apparent positions on SAR images.

D. Inversion of the system

Let $\boldsymbol{X}$ be the target parameter vector and $\boldsymbol{Y}$ the measurement vector. $\boldsymbol{X}$ is defined by:

$$\boldsymbol{X} = (x_i)_{i\in[1,5]} = \left(X, Y, V, A, \theta_{target}\right) \quad (12)$$

$\boldsymbol{Y}$ is given by:

$$\boldsymbol{Y} = (y_i)_{i\in[1,3\times N]} = \left(i_1 \dots i_N, j_1 \dots j_N, \alpha_1 \dots \alpha_N\right) \quad (13)$$

The moving target trajectory is obtained by estimating the target parameter vector $\widehat{\boldsymbol{X}}$ as follows:

$$\widehat{\boldsymbol{X}} = \operatorname{argmin}\left(\sum_{n=1}^{N}\sum_{m=1}^{3} f_{m,n}^2(\boldsymbol{X},\boldsymbol{Y})\right) \quad (14)$$

Where f_{1n}, f_{2n} and f_{3n} are the three equations in (10) for the nth sub-aperture image. $\widehat{\boldsymbol{X}}$ is estimated by the Least Mean Squares method, using the Levenberg-Marquardt algorithm [30].

IV. MATHEMATICAL ANALYSIS

In this section, we study the method robustness using realistic synthetic moving target. Using a perfect synthetic aircraft trajectory, we perform a mathematical analysis of the robustness and then we invert synthetic target trajectories to validate this analysis.

A. Generation of a perfect synthetic aircraft trajectory

In order not to take into account the aircraft turbulences, we generate a perfect synthetic aircraft with characteristics close to our dataset for system validation. The characteristic of the simulation are given in Table II.

TABLE II
SYNTHETIC AIRCRAFT TRAJECTORY PARAMETERS

Symbol	Quantity	Value
ρ_r	Range resolution	0.25 m
ρ_a	Azimuth resolution	0.002°
λ	Center wavelength	3 cm
N	Number of images used for the inversion	Variable
$\Delta\theta$	Angle between two images	2°
ΔT	Time interval between two images	$\cong 1.4s$

B. Mathematical study of the Robustness

The system (10) is a non-linear system, so the estimate of the output parameters $\widehat{\boldsymbol{X}}$ cannot be analytically given with respect to the measurements $\mathbf{Y}$. This system can be modelled by an implicit function as follows:

$$f(\boldsymbol{X},\boldsymbol{Y}) = 0 \tag{15}$$

A development of (15) at the vicinity of the solution $\widehat{\boldsymbol{X}}$ of the system leads to:

$$\boldsymbol{M_y}\boldsymbol{\delta Y} = \boldsymbol{M_x}\boldsymbol{\delta X} \tag{16}$$

$\boldsymbol{M_x}$ represents the matrix of first partial derivatives of the inversion system (10) with respect to $\mathbf{X}$ and evaluated in $\widehat{\boldsymbol{X}}$:

$$\boldsymbol{M_x} = \left(\frac{\partial f_i}{\partial x_j}(\widehat{\boldsymbol{X}},\boldsymbol{Y})\right)_{i\in[1,3N],\, j\in[1,5]} \tag{17}$$

$\boldsymbol{M_y}$ represents the matrix of first partial derivatives of the inversion system (10) with respect to measurements $\mathbf{Y}$ and evaluated in $\widehat{\boldsymbol{X}}$**:**

$$\boldsymbol{M_y} = \left(\frac{\partial f_i}{\partial y_j}(\widehat{\boldsymbol{X}},\boldsymbol{Y})\right)_{i\in[1,3N],\, j\in[1,3N]} \tag{18}$$

From the expression (16), we obtain:

$$\boldsymbol{\delta X} = \left(\boldsymbol{M_x}^{\boldsymbol{T}}\boldsymbol{M_x}\right)^{-1}\boldsymbol{M_x}^{\boldsymbol{T}}\boldsymbol{M_y}\boldsymbol{\delta Y} \tag{19}$$

The analytical expressions of $\boldsymbol{M_x}$ and $\boldsymbol{M_y}$ are very complex. In order to study the robustness of the method, we first analyse the inversibility of $\boldsymbol{H_x} = \boldsymbol{M_x}^{\boldsymbol{T}}\boldsymbol{M_x}$, by computing the condition number of $\boldsymbol{H_x}$.This condition number is given by :

$$C_{\boldsymbol{H_x}} = \|\boldsymbol{H_x}\|\left\|\boldsymbol{H_x}^{-1}\right\| \tag{20}$$

In numerical analysis, we consider that the numerical stability of the system will be guaranteed only if $C_{\boldsymbol{H_x}}$ is less than a limit value C_{lim} which is linked to the machine accuracy eps:

$$C_{lim} = \frac{1}{\sqrt{eps}} \tag{21}$$

Fig. 6 shows the evolution of $C_{\boldsymbol{H_x}}$ with respect to the total angular span used to solve the system for two different moving target models: the first one is a model of a moving target with constant acceleration and colinearity constraint with 5 unknown (X,Y,V,A,θ_{target}), and the second is a model with constant velocity (X,Y,V,θ_{target}). We generate independent data, so that the interval angle between two images is strictly equal to the integration angle for each image. As we want an azimuth resolution corresponding to the resolution of our real data (which is equal to 0.5m, approximately), the corresponding interval angle between two images is given by:

$$\Delta\theta \cong \frac{\lambda}{2\rho_a D_0} \tag{22}$$

In this case, $\Delta\theta$ is approximately equal to 2°, so we choose an interval angle equal to 2°.

The x axis represents the total angular span $\Delta\theta_{max}$ used for inversion, given by $\Delta\theta_{max} = N\Delta\theta$. We test different values of $\Delta\theta_{max}$ ranging from 4° to 180°. We clearly see that the condition number is too high for the model (X,Y,V,A,θ_{target}), the value of $C_{\boldsymbol{H_x}}$ is less than C_{lim} only for $\Delta\theta_{max} > 100°$. We tested other types of trajectories and we always obtained similar results. So the robustness of the method is not guaranteed with this model. By contrast, from a certain angular span, we see that the condition number is sufficiently low for the model (X,Y,V,θ_{target}). The numerical stability seems to be guaranteed with this model, but we want to validate it on realistic measurement errors. From now on we only study the model (X,Y,V,θ_{target}).

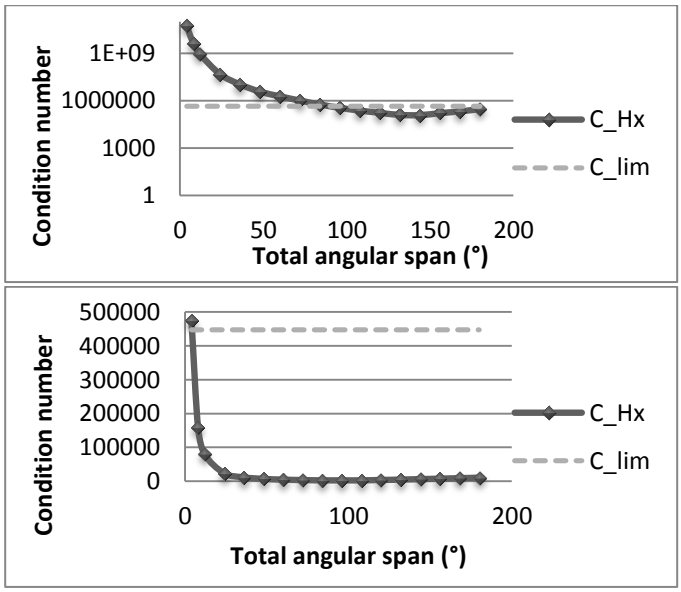

Fig. 6. Evolution of the condition number $\boldsymbol{C_{H_x}}$ with respect to the total angular span $\Delta\theta_{max}$. Top: results with the model (X,Y,V,A,θ_{target}). Bottom: results with the model (X,Y,V,θ_{target}).

C. Inversion with synthetic moving targets

In this section, we validate the inversion system and the study of the robustness. We first compute apparent trajectories of synthetic moving targets, and then we test two different types of perturbations. In the first case, we simulate a moving target trajectory which corresponds to the models (with constant velocity) and we add Gaussian noise to the

computed apparent characteristics (i,j,α) to test the sensitivity of the inversion to measurement errors. For (i,j), we add a zero mean noise with σ=1m, and for α we add a noise corresponding to a 1m error on the target defocusing length. In the second case, we simulate a moving target trajectory with no measurement errors, but with a sinusoidal perturbation with σ≅0.7m. So the real trajectory does not fit the model. In this case, we test the sensitivity of the inversion to deviations from the moving target models. This second perturbation and the corresponding apparent trajectory are represented in Fig. 7.

The moving target trajectories are then estimated with the above-described methodology, given different angular spans. The normal configuration is a moving target with V=5m.s^{-1}, V_S=120m.s^{-1}, the incidence *inc*=60° and D_0=5000m. We test separately the impact of variation of V, V_S, *inc* and D_0. So for each test, only one parameter is changed. We compute the RMS differences between the estimated trajectory and the synthetic ground truth. We present the results in the table III obtained with the (X,Y,V,θ_{target}) model.

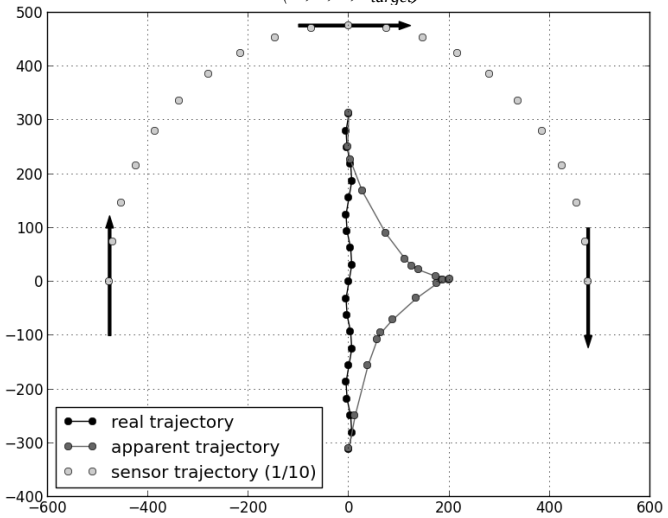

Fig. 7. Representation of a synthetic target trajectory (black) moving towards North with a sinusoidal perturbation, and its corresponding apparent trajectory (dark grey). The positions of the sensor are represented in light grey.

The results are evaluated on four parameters: $\Delta\theta_{lim}$ represents the angular span beyond which the RMS differences are less than *20m*, that is the minimal angular span needed to obtain a non aberrant trajectory, t_{lim} is the time interval corresponding to $\Delta\theta_{lim}$, m_{RMS} and σ_{RMS} represent the mean and the standard deviation of the RMS differences for the angular spans beyond $\Delta\theta_{lim}$.

These results confirm the mathematical analysis of the robustness. We see that from a certain angular span (depending on the parameters), the estimated trajectory is close to the ground truth. We also notice that the method is highly sensitive to deviation from the moving target model, because we need large angular spans to obtain accurate reconstructions in the second case. Finally, we can see that the influence of the tested parameters (sensor velocity, incidence, range…) on the reconstruction is limited. One can conclude that the main limiting factor of this reconstruction method is the accuracy of the constant velocity model of the moving target.

TABLE III
STATISTICS ON THE RMS DIFFERENCES BETWEEN THE ESTIMATED TRAJECTORY AND THE SYNTHETIC GROUND TRUTH, GIVEN DIFFERENT TARGET VELOCITIES AND ACQUISITION PARAMETERS.

	Gaussian noise			
	$\Delta\theta_{lim}$ (°)	t_{lim} (s)	m_{RMS} (m)	σ_{RMS}(m)
Normal	20	13.8	1.93	2.61
$V = 10m.s^{-1}$	20	13.8	1.84	2.39
$V_S = 60m.s^{-1}$	24	16.5	2.21	3.25
$inc = 45°$	16	11	1.96	2.73
$D = 20000m$	32	22	2.34	3.32
	Sinusoidal perturbation			
	$\Delta\theta_{lim}$ (°)	t_{lim} (s)	m_{RMS} (m)	σ_{RMS}(m)
Normal	60	41	2.37	2.71
$V = 10m.s^{-1}$	60	41	2.39	2.75
$V_S = 60m.s^{-1}$	72	50	1.89	1.95
$inc = 45°$	60	41	2.48	2.80
$D = 20000m$	72	50	2.09	2.26

V. EXPERIMENTAL RESULTS ANALYSIS

In this section, we present some results concerning real moving target tracking around the city of Nîmes and Istres (two cities in the South of France). We first focus on Istres data and on the moving target presented in Fig. 1. We applied the inversion algorithm to calculate the moving target trajectory and to compare it to the GPS truth. Fig. 8 shows the RMS differences between the estimated trajectory of the real moving target on Istres data and its GPS position. The x axis represents the index of the first image used to solve the system. Since the sensor is moving along the circular trajectory, this number is linked with the difference of orientation between sensor velocity and target velocity. The y axis represents $\Delta\theta_{max}$. We tested again the two different moving target models: the one with constant velocity (see Fig. 8, left) and the one with constant acceleration (see Fig. 8, right).

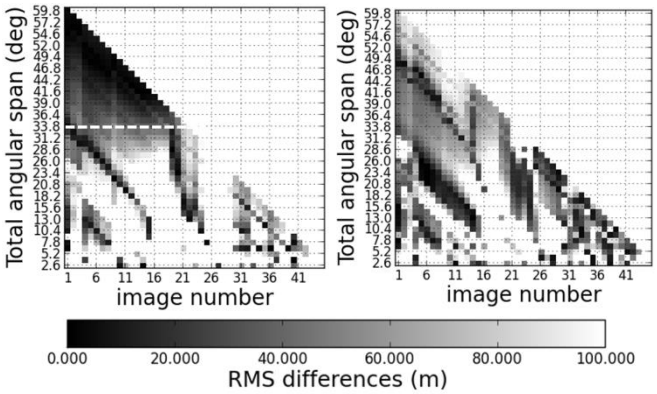

Fig. 8. RMS differences between the estimated trajectory of a real moving target around the city of Istres and its ground truth (GPS data). On the left is the result with the constant velocity model and on the right is the result with

the constant acceleration model. The red line on the left represent the angular span at which the trajectory estimation is close to the GPS truth.

These results show that from a certain angular span (white line, see Fig. 8), the estimated trajectory is close to the ground truth when we use a constant velocity model. It is not the case if we add the acceleration as a degree of freedom, which confirms the results of the mathematical analysis of the robustness. Fig. 9, which represents vertical cross-sections of the first column of the two images presented in Fig. 8, highlights this observation.

One of the configurations of Fig. 8 is used to show an example of trajectory reconstruction of the moving target (see Fig. 10). We took a time interval ΔT_{max} between the two farthest images equal to 37s (corresponding to a total angular span $\Delta\theta_{max}$ equal to 50° approximately) to compute this trajectory. The red dots represent the result of the trajectory computation and the green dots represent the apparent trajectory of the moving target, *i. e.* the apparent position of the moving target on all the images, but projected on a single image. As the line of sight changes from one image to the other, the delocalization direction changes leading to a real trajectory shorter than the apparent one.

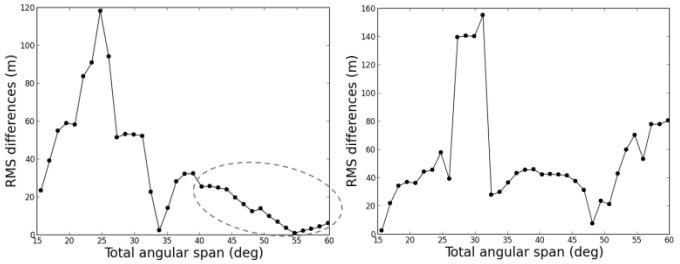

Fig. 9. RMS differences between the estimated trajectory and the GPS data with respect to the angular span. On the left is the result with the constant velocity model and on the right is the result with the constant acceleration model. We see that with the constant velocity model, the estimations are close to the GPS data for angular spans beyond 40°.

We then compare the calculation result with the GPS data by computing RMS differences between the two trajectories. The moving target trajectory reconstruction is very accurate. The average position RMS error on the whole target trajectory is less than $5m$. The error of the velocity is $0.11m.s^{-1}$, which correspond to an average error about 2%. Concerning the acceleration and orientation errors, they are very low ($0.04m.s^{-2}$ and 1.28°, respectively).

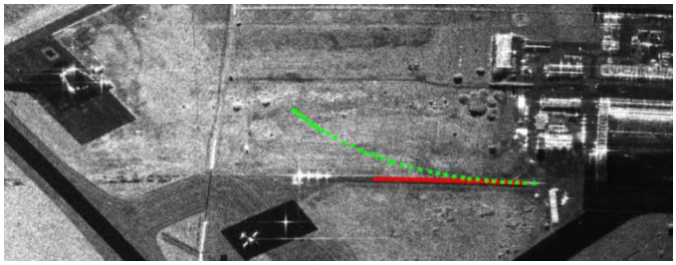

Fig. 10. Trajectory reconstruction for a real known trajectory (with ground truth) near the Istres airport. The red dots represent the result of the trajectory computation, and the green dots represent the apparent trajectory of the moving target. The moving target is a Renault Master travelling at an average speed of $4m.s^{-1}$.

Fig. 11 shows the trajectory of the moving target obtained around the city of Nîmes concerning the moving target with unknown movements. We took a time interval ΔT_{max} between the two farthest images equal to $28s$ (corresponding to a total angular span $\Delta\theta_{max}$ equal to 45° approximately) to compute this trajectory.

The green dots represent the apparent trajectory of the moving target during the time ΔT_{max}, *i. e.* the coordinates of the moving target center in all the SAR images used for the trajectory calculation. The coordinates of the moving target center is obtained by using the measurement methodology described on the section II. We projected all these coordinates on a single image for visualisation. The measured velocity of the moving target is almost constant and equal to $37km/h$. Furthermore, the target is close to the railway (green dotted lines), the average position RMS error on the whole target trajectory is around 15m. The red dots represent the result of the trajectory computation. All these characteristics are consistent with a train arrival in the Nîmes station (red circle).

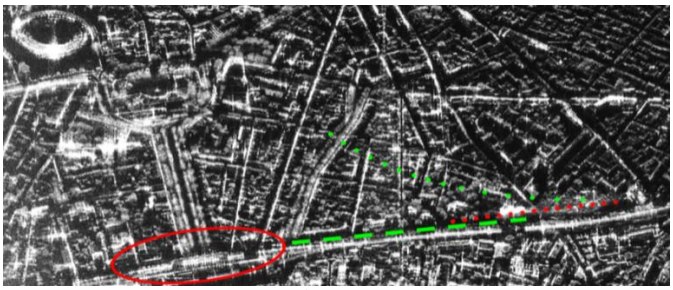

Fig. 11. Trajectory reconstruction for a real unknown trajectory. Red circle is the train station of the city of Nîmes. The red dots represent the result of the trajectory computation, and the green dots represent the apparent trajectory of the moving target. The green (dashed) line represents the railway.

VI. Road Network Constraint

In order to encompass the instability responses of the constant acceleration model, we have tried to add an orientation constraint given by the road network [31]. The reconstruction is performed using the moving target model with constant acceleration. 3 different moving target orientations are tested, and the method automatically selects the target orientation that minimizes $\Phi(\boldsymbol{X},\boldsymbol{Y})$ given by (13). Results are shown on Fig. 12. They are obtained on the Istres dataset.

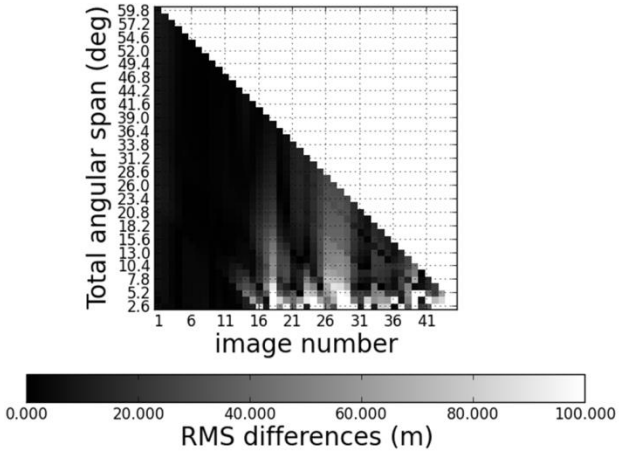

Fig. 12. RMS between the estimated trajectory of a real moving target around the city of Istres and its ground truth (GPS data), with a model containing an information about the road network.

These results show that if we use the road directions (in urban context), the trajectory estimation is very precise, even with small angular spans. As the results are obtained with the constant acceleration model, the trajectory reconstruction method is efficient for more complex movements.

VII. Conclusion

This paper presents a novel methodology to reconstruct moving target trajectories from their apparent coordinates in a set of SAR images acquired along a circular trajectory in a monosensor spotlight mode. This method consists in inverting a *3N* equation system, *N* being the number of used images. The ambiguity between azimuthal position and radial velocity of the moving target is solved.

The apparent coordinates measurements are given by an autofocus and relocation method. We do not work on automatic target detection but we could have used the work described in [13] or in [22]. Results on real data have shown the efficiency of this measurement method in strong clutter environment or in urban context (especially in Nîmes [28]), which is a contribution compared to existing methods [13,19].

A validation with synthetic aircraft and target trajectories was carried out, testing two different moving target models: one with a constant velocity and one with a constant acceleration. This validation has highlighted the sensitivity of the method when considering a moving target model with acceleration and its stability with the constant velocity model.

Results on real moving targets trajectory reconstruction are shown around the city of Istres and Nîmes. The computation of the RMS differences confirms the results obtained on synthetic trajectories and proves the efficiency of the method with the constant velocity model for an angular span larger than 35°.

One can conclude that the reconstruction of a real trajectory based on monosensor measurements on SAR data acquired along a circular trajectory is possible under several hypotheses:

- If the road network is not used, we have to choose the moving target model with constant velocity and a large enough angular span to retrieve precisely the moving target trajectory. It induces a tradeoff between the angular span, the precision of the reconstruction and the constant velocity hypothesis.

- If the road network is known, it can be used to encompass the instabilities using the constant acceleration model by adding orientation constraints on the system. In this case good results are obtained even for small angular spans. Further work should be done to study the best way to implement the road information in the inversion scheme.

Acknowledgment

The authors would like to thank the RAMSES NG team (O. Ruault du Plessis, R. Baqué, G. Bonin, P. Fromage, and D. Heuzé) for having acquired the data around the city of Istres, the pilots for having performed the circular path, and the anonymous reviewers for their constructive comments.

References

[1] I. G. Cumming and F. H. Wong, *Digital Processing of Synthetic Aperture Radar Data, Algorithms and Implementation*. Boston, MA: Artech House, 2005.

[2] R. K. Raney, "Synthetic aperture imaging radar and moving targets," *IEEE Trans. Aerosp. Electron. Syst*., vol. AES-7, no. 3, pp. 499-505, May 1971.

[3] R. Deming, J. Schindler, and L. Perlovsky, "Multitarget/Multisensor Tracking using only Range and Doppler Measurements," *IEEE Transactions on Aerospace and Electronic Systems*, vol. 45, no. 2, 2009.

[4] F. R. Dickey, M. Labit et F. M. Staudaher, «Development of Airborne Moving Target Radar for Long Range Surveillance,» *IEEE Trans. Aerosp. Electron. Syst.*, vol. 27, no. 16, pp. 959-972, 1991.

[5] J. Ward, *Space-time adaptive processing for airborne radar*. MIT Lincoln Lab., Lexington, MA, Tech. Rep. 1015, Dec. 1994.

[6] S. Barbarossa, "Detection and imaging of moving objects with synthetic aperture radar. Part 1: optimal detection and parameter estimation theory," IEE Proc-F, vol. 139, no. 11, pp. 79-88, 1992.

[7] A. Budillon, V. Pascazio, and G. Schirinzi, "Estimation of radial velocity of moving targets by along-track interferometric SAR systems," *IEEE Geosci. Remote Sens. Lett*, vol. 5, no. 3, pp. 349-353, Jul. 2008.

[8] R. Deming, "Along-Track Interferometry for Simultaneous SAR and GMTI: Application to Gotcha Challenge Data," in *Algorithms for Synthetic Aperture Radar Imagery XVIII, Proceedings of SPIE*, vol. 8051, no. 80510P, may 2011..

[9] S. R. J. Axelsson, "Position correction of moving targets in SAR imagery," *Proc. SPIE*, vol. 5236, pp. 80-92, Jan. 2004.

[10] J. J. Sharma, C. H. Gierull, and M. J. Collins, "The influence of target acceleration on velocity estimation in dual-channel SAR-GMTI," *IEEE Trans. Geosci. Remote Sens.*, vol. 44, no. 1, pp. 134-147, Jan. 2006.

[11] G. Bonin and P. Dreuillet, "The airborne SAR system SETHI: Airborne microwave remote sensing imaging system," in *Proc. EUSAR*, Friedrichshafen, Germany, 2008, pp. 1-4.

[12] R. Baqué and P. Dreuillet, "The airborne SAR-system : RAMSES NG Airborne microwave remote sensing imaging system," *in IET International Conference on Radar Systems (Radar 2012)*, Glasgow, UK, 2012, pp. 1-4.

[13] J. R. Fienup, "Detecting moving targets in SAR imagery by focusing," *IEEE Trans. Aerosp. Electron. Syst.*, vol. 37, no. 3, pp. 794-809, Jul. 2001.

[14] T. Sparr, "Time-frequency signature of a moving target in SAR images," in *Proc. RTO-MAP-SET*, 2004, pp. 1-8.

[15] R. P. Perry, R. C. Dipietro and R. L. Fante, "SAR imaging of moving targets," *IEEE Trans. Aerosp. Electron. Syst.*, vol. 35, no. 1, pp. 188-200, Jan. 1999.

[16] P. A. C. Marques and J. M. B. Dias, "Velocity estimation of fast moving targets using a single SAR sensor," *IEEE Trans. Aerosp. Electron. Syst.*, vol. 41, no. 1, pp. 75-89, Jan. 2005.

[17] V. C. Chen, "Time-frequency analysis of SAR image with ground moving targets," *Proc. SPIE*, vol. 3391, pp. 295-302, Apr. 1998.

[18] M. J. Minardi, L. A. Gorham and E. G. Zelnio, "Ground moving target detection and tracking based on generalized SAR processing and change detection (invited paper)," *Algorithms for Synth. Aperture Radar Imagery XII*, vol. 5808, No. 1, pp. 156-165, 2005.

[19] J. K. Jao, "Theory of synthetic aperture radar imaging of a moving target," IEEE Trans. Geosci. Remote Sens., vol. 39, no. 9, pp. 1984-1992, 2001.

[20] M. Kirscht, "Detection and imaging of arbitrarily moving targets with single-channel SAR," *Proc. Inst. Elect. Eng.-Radar Sonar Navig.*, vol. 150, no. 1, pp. 7-11, Feb. 2003.

[21] K. Ouchi, "On the multilook images of moving targets by Synthetic Aperture Radars,"*IEEE Trans. Antenn. Propagat.*, vol. 3, no. 8, pp. 823-827, Aug. 1985.

[22] M. Kirscht, "Detection and focused imaging of moving objects evaluating a sequence of single-look SAR images," in *Proc. 3rd Int. Airborne Remote Sens. Conf. Exhib.*, Copenhagen, Denmark, Jul. 1997, vol. I, pp. 393-400

[23] J. M. B. Dias and P. A. C. Marques, "Multiple moving targets detection and trajectory parameters estimation using a single SAR sensor," *IEEE Trans. Aerosp. Electron. Syst.*, vol. 39, no. 2, pp. 604-624, Apr. 2003.

[24] T. Itoh, H. Sueda and Y. Watanabe, "Motion compensation for ISAR via centroid tracking," IEEE Trans. Aerosp. Electron. Syst., vol. 32, pp. 1191-1197, 1996.
[25] M. Soumekh, "Reconaissance with slant plane circular SAR imaging," *IEEE Trans. Image Process.*, vol. 5, no. 8, pp. 1252-1265, Aug. 1996.
[26] L. Perlovsky, R. Ilin, R. Deming, R. Linehan and F. Lin, "Moving target detection and characterization with circular SAR," in *IEEE Radar Conference*, Washington, DC, 2010, pp. 661-666.
[27] D. Henke, C. Magnard, M. Frioud, D. Small, E. Meier and M. E. Schaepman, "Moving-Target Tracking in Single-Channel Wide-Beam SAR," *IEEE Trans. Geosci. Remote Sens.*, vol. 50, no. 11, pp. 4735 - 4747, 2012.
[28] J.B. Poisson, H. Oriot, F. Tupin, "Performances analysis of moving target tracking in circular SAR," in *Proc. IRS*, Dresden, Germany, 2013, pp. 1-6.
[29] J. B. Poisson, H. Oriot, F. Tupin, "Moving target tracking using circular SAR imagery," in *Proc. EUSAR*, Nuremberg, Germany, 2012, pp. 1-4.
[30] B. W. Marquardt, "An algorithm for least-squares estimation of nonlinear parameters," *SIAM J. Appl. Math*, vol. 11, pp. 431-441, 1963.
[31] P. A. C. Marques, "SAR-MTI improvement using *a-priori* knowledge of the road network," in *Proc. Eur. Radar Conf.*, Oct. 2010, pp. 244-247.

Jean-Baptiste Poisson was born in Versailles, France, in 1986. He received the engineer degree from Ecole Supérieure d'Optique, Palaiseau, France, in 2010, and the the Ph.D. degree in signal and image processing from Télécom ParisTech, Paris, France, in 2013.

He is currently at ONERA, The French Aerospace Lab, Palaiseau, France, in the Electromagnetic and Radar Department. His research interests include focusing and tracking techniques for moving objects in SAR applications, SAR processing, numerical optimization, probabilistic modeling, signal and image processing.

Hélène M. Oriot was born in Talence, France, in 1968. She received the engineer degree from Ecole Centrale Paris, Paris, France, in 1991, the M.Sc. degree in ocean engineering from the Massachusetts Institute of Technology, Cambridge, in 1992, and the Ph.D. degree in computer science from the Institut National Polytechnique de Toulouse, Toulouse, France, in 1996.

Since 1996, she has been with ONERA, The French Aerospace Lab, Palaiseau, France, first, in the Image Processing Department as a Scientist, where she was involved with 3-D reconstruction from stereo-optical imagery, and, then, in the Electromagnetic and Radar Department in 2005. Her research interests include 3-D reconstruction using SAR data from airborne sensors, interferometry, SAR processing, and airborne SAR sensor calibration.

Florence Tupin (M'04–SM'07) received the Engineer degree in 1994 and the Ph.D. degree in signal and image processing from École Nationale Supérieure des Télécommunications (ENST), Paris, France, in 1997. She is currently a Professor with Telecom Paris-Tech, France.

From 1997 to 1998, she worked with SAGEM in fingerprint recognition. Since November 1998, she has been Associate Professor and then Professor of signal processing and computer vision at Telecom ParisTech in the Image and Signal Processing Department. Her research interests are image analysis and interpretation, three-dimensional reconstruction, Markov random fields, and synthetic aperture radar, especially for urban remote sensing applications. In 2007, Dr. Tupin was chair of the Urban Remote Sensing Joint Event held in Paris.

Since 2003 she has been a member of the technical committees Pattern Recognition in Remote Sensing of the International Association for Pattern Recognition (IAPR), and URBAN, the biennial GRSS/ISPRS Joint Workshops on Remote Sensing and Data Fusion over Urban Areas from 2004 to 2006. From 2005 to 2007, she was Associate Editor of the French journal *Signal Processing*. She currently serves as an Associate Editor of IEEE TRANSACTIONS ON GEOSCIENCE AND REMOTE SENSING.